RSC Advances

A selenium-confined porous carbon cathode from silk cocoon for Li-Se battery application

Journal:	*RSC Advances*
Manuscript ID	RA-ART-09-2015-019000.R1
Article Type:	Paper
Date Submitted by the Author:	12-Oct-2015
Complete List of Authors:	Jia, Min; Clean Energy & Advanced Materials, Faculty of Materials and Energy, Southwest University, Mao, Cuiping; Clean Energy & Advanced Materials, Faculty of Materials and Energy, Southwest University, Niu, Yu-Bin; Institute for Clean Energy and Advanced Materials, Southwest University, Hou, Jun; Southwestern University, Institute of Clean Energy & Advanced Materials Liu, Sangui; Clean Energy & Advanced Materials, Faculty of Materials and Energy, Southwest University, BAO, SHU-JUAN; Institute for Clean Energy & Advanced Materials, Jiang, Jian; Institute of Clean Energy & Advanced Materials, Xu, Mao-Wen; Institute of Clean Energy & Advanced Materials, Lu, Zhisong; Southwest University, Institute for Clean Energy & Advanced Materials
Subject area & keyword:	Electrochemistry < Physical

JournalName RSCPublishing

COMMUNICATION

A selenium-confined porous carbon cathode from silk cocoon for Li-Se battery application

Cite this: DOI: 10.1039/x0xx00000x

Min Jia[a,b], Cuiping Mao[a,b], Yubin Niu[a,b], Junke Hou[a,b], Sangui Liu[a,b], Shujuan Bao[a,b], Jian Jiang[a,b], Maowen Xu[a,b,]* and Zhisong Lu[a,b,]*

Received 00th January 2012,
Accepted 00th January 2012

DOI: 10.1039/x0xx00000x

www.rsc.org/

Composite of selenium (Se) and rich porous carbon materials (PCMs) with mesopores from silk cocoon is explored as cathode for lithium-selenium (Li-Se) batteries for the first time. The elemental selenium is homogeneously dispersed inside the mesopores of PCMs by a melt-diffusion method based on the analyses. The synthetic PCMs/Se composite can effectively suppress the dissolution of the active material and maintain mechanical stability. In the case of Li-Se batteries, it delivers a reversible capacity of more than 230 mAh g^{-1} after 510 cycles at 2 C. The remarkable electrochemical performance may benefit from the favorable conductivity and the porous structure of the carbon material as host matrixes.

The increasing need for the high energy density of the lithium secondary battery has attracted more and more extensive attention because of the energy crisis and environmental protection problem.[1-3] Lithium-ion batteries (LIBs) are the viable option in response to the above problem that could be used as energy storage devices for renewable sources. In the past two decades, the Li-ion batteries have been widely used based on their increased energy density and - long life cycle.[4-5] However, the existing Li-ion batteries could only afford a low energy density which caused by that the majority of battery active substances were the heavy metals or transition metal oxide. And the heavy host lattices required for Li-ion intercalation fundamentally limits the capacity.[6] Therefore, a new generation of cathode materials which could afford high capacity and energy density is urgently needed. Among various kinds of rechargeable batteries, the Li-S batteries have been studied as the excellent system owe to their high theoretical energy density (2600 Wh kg^{-1}) and specific capacity (1675 mAh g^{-1}).[7] Although the preponderances were shown as above, the application of Li-S batteries still face tremendous challenges on account of the insulating characteristic of S (10^{-30} S cm^{-1}) and the solubility of polysulfide intermediates during cycling.[8]

Selenium (Se) has been proposed to the most promising cathode material not only about the similar redox mechanism and the location of the same group to sulfur, but also about the higher electrical conductivity (10^{-5} S cm^{-1}) and comparable volumetric capacity (3253 Ah L^{-1} based on 4.82 g cm^{-3}).[9-10] However, the fast capacity fading and poor cycle performance caused by dissolution issue of high-order polyselenides still are the serious problems which have to been faced with.[11]

Recently, several methods have been taken to trap the polyselenides by encapsulating Se in various porous carbons [12-16], conductive polymers [17], graphene materials [18-19] or TiO_2 [20]. Of them, it is deserved to be mentioned that Yang et al. [21] had prepared the ordered mesoporous carbon-Se composite by a facile melt diffusion route. In that work, they confined selenium in the form of cyclic Se_8 molecules in the common mesoporous carbon (CMK-3) and the obtained composite is stable due to the confinement of the mesoporous structure and the strong interaction between the Se and carbon. The

other favorable strategy to prepare the porous carbon material is using polypyrrole (Ppy) nanofibers as the precursor with the activation process which is conducted by Zhang et al. [22] The synthesized composite continued the cross-linked structure which had showed in the carbon material carbonized from PPy nanofibers, therefore it exhibited a superior capacity.

In this work, we employed a simple method to prepare PCMs from silk cocoon, and N_2 absorption–desorption isotherm of the PCMs suggests that its specific surface area as high as 2442.1 $m^2 g^{-1}$. To our knowledge, there is no report on the application of PCMs from silk cocoon as host matrixes for Li−Se batteries. Accordingly, we choose PCMs/Se composite prepared by simple melt infiltration method as the cathode material. The specific capacity and cycle performance of Li–Se batteries are significantly enhanced with a reversible capacity of more than 230 mAh g^{-1} after 510 cycles at a current density of 2 C.

Experimental Section

Materials preparation

Preparation of PCMs from silkworm cocoon: The silkworm cocoon were firstly washed with sodium carbonate solution and deionized water several times, and dried at 60 ℃ for nearly 4 hours in the vacuum oven before next step. To derive the carbon material (CMs), the pretreated silkworm cocoon were carbonized at 600 ℃ for 2 h under a flowing Ar atmosphere in a tubular furnace with a heating rate of 2 °C min^{-1}. And then the obtained CMs was grinded with KOH with the mass ratio (w_c:w_{KOH}=1:2) for about 15 min. After that, the mixtures were heated at 300 °C for 1.5 h and at 750 °C for 2 h under Ar atmosphere with a heating rate of 5 °C min^{-1}. The derived samples were washed with 1 M HCl to dissolve the impurity and then deionized water for several times and dried at 80 °C for 12 h.

Preparation of PCMs encapsulating Se Composites (PCMs/Se): The as-prepared PCMs sample and Se were mixed well with the mass ratio of w_c:w_{Se}=2:3 in a quartz mortar. The mixture was heated to and maintained at 260 ℃ for 2 h with the simple melting diffusion way to obtain the PCMs/Se composite at a heating rate of 5 ℃ min^{-1} under Ar atmosphere. The obtained PCMs/Se composite were characterized in detail what follows in the passage. For comparison, different mass ratios of C/Se had been experimented. The electrochemical performance of three typical mass ratios w_c:w_{Se}=1:1, w_c:w_{Se}=2:3 and w_c:w_{Se}=1:2 were shown in Fig.S1. We choose the optimized ratio of C/Se: w_c:w_{Se} =2:3 to obtain the best performance.

Material characterization

Morphological observations were characterized by field-emission scanning electron microscopy (FESEM, JSM-7800N) and transmission electron microscopy (TEM, JEM-2100). The crystal structures of the as-prepared products were examined by X-ray diffractometer (Maxima-X XRD-7000) with Cu K-alpha radiation (λ=1.5406 nm). The data were collected over a 2θ range between 10° and 80°. Raman tests were conducted using a HORIBA Scientific LabRAM HR Raman spectrometer system with a laser wavelength of 532.4 nm. X-ray photoelectron spectroscopy (XPS) measurements were conducted using a Thermo Scientific ESCALAB 250Xi electron spectrometer. TGA was used to determine the weight contents of Se which was carried out by thermogravimetric analyzer (TGA, Q50). The pore size distribution and nitrogen adsorption−desorption isotherms were measured by Quadrasorb evo 2QDS-MP-30 (Quantachrome Instruments, USA).

Electrochemical measurements

To evaluate the electrochemical properties of the PCMs/Se composite cathodes, the electrodes were fabricated by coating Al foil with a slurry containing the active material (80 wt%), carbon black (10 %), and sodium alginate (SA) binder (10 wt%) dissolved in deionized water. The coated electrodes were dried at 60 °C for 15 h in vacuum. CR3025 coin cells were used as the electrochemical tests and Li foil was utilized as the counter electrode. The electrolyte was 1 M $LiPF_6$ dissolved in a mixture of ethylene carbonate (EC) and diethyl carbonate (DEC) with a volume ration of 1:1. The cells were assembled in an argon-filled glovebox and then aged for about 6 hours before charge-discharge. Charge–discharge characteristics were galvanostatically tested between 1.0 V~3.0 V (vs. Li/Li^+) at room temperature using a Land instruments testing system.

Results and Discussion

FESEM was used to examine the morphologies of the as-prepared CMs, PCMs and PCMs/Se, respectively. As shown in Fig. 1a and b, it can be observed that the CMs is composed of large fragment-like particles and its magnified SEM image(Fig. 1b) shows the average diameter of it is around 1 μm. The geometric morphologies of the PCMs were shown in Fig. 1(c-d) and the representative overview of it is similar to the sample of CMs. It may because that after activation the structure of CMs had not been changed but only with better mesoporous structure. Fig.1 (e-f) depicts the morphologies of PCMs/Se composite and the size of it is uniform with the Se fusing into the porous material (PCMs). Obviously, there was not obvious different block material observed from the magnified SEM image (Fig. 1f), which may suggest that Se was well impregnated into PCMs.

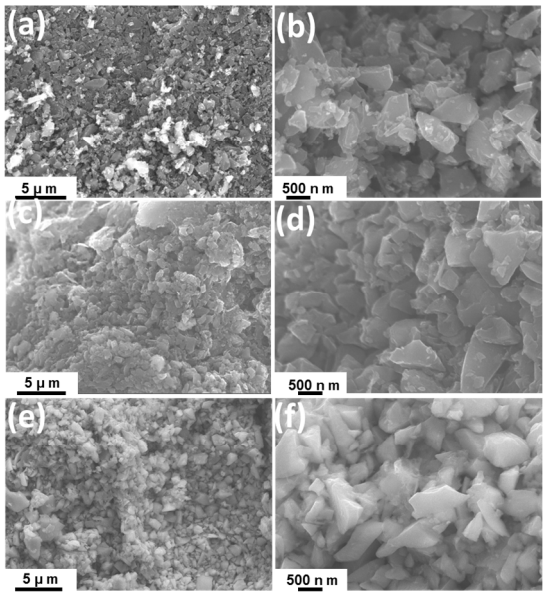

Figure 1 SEM images of (a), (b) CMs; (c), (d) PCMs; (e), (f) PCMs/Se.

The CMs, PCMs and PCMs/Se samples were further characterized by TEM. As shown in Fig. 2a, multilayer structures could be found for the CMs sample from the TEM image (Fig. 2a). Further enlarged TEM image (Fig. 2b) indicates that the CMs were composed of highly disordered macropores and its surface looks like slack. After further KOH activation, the surface of PCMs becomes slacker and keeps intact with the CMs in a rough feature (Fig. 2c). The representative TEM image (Fig. 2d) reveals that a large amount of pores are homogeneously dispersed on the surface of PCMs. In Fig. 2(e-f), the morphology of PCMs/Se composite was illustrated. The rough surface was obviously seen from Fig. 2(e), which suggesting that Se successfully fused into the pores of PCMs. Moreover, it is clearly that the (101) crystal plane of selenium could be found in the composite of PCMs/Se in the HRTEM observation (Fig. 2f), which is in the corresponding with the XRD pattern shown behind. The SEM image and elemental maps of PCMs/Se composite are shown in Fig. 2(g-j). It is clearly to be seen that the similar intensity of the carbon and selenium could be found in the figure, which indicating that Se has a highly dispersed state in PCMs/Se composite.[11] This corroborates well with SEM and TEM observation.

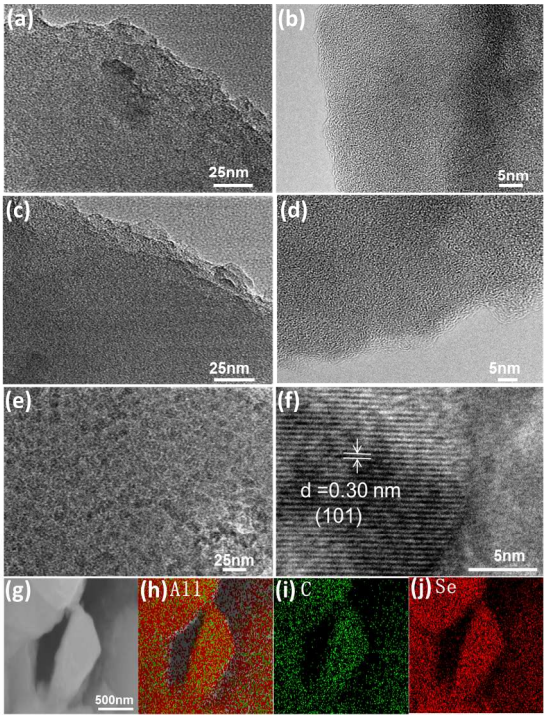

Figure 2 TEM images of (a), (b) CMs; (c), (d) PCMs; (e), (f) PCMs/Se. (g) SEM image, and (h-j) elemental mappings of PCMs/Se composite samples.

XRD patterns of Se (red), CMs (black), PCMs (blue) and PCMs/Se (purple) samples are presented in Fig. 3(a). The broad reflection of about 24° of PCMs, which is attributed to amorphous characteristic of the as-prepared PCMs. [11] For Se, which was heated to 260℃ and held for 2 hours, there are several peaks at 23.5° (100), 29.7° (101), 41.3° (110), 43.6°(102), 45.4° (111), 51.8° (201), 55.7° (112), and 61.5° (202), which are consistent with the diffraction peaks of the trigonal phase of Se (JCPDS 06-0362).[23] As shown in Fig. 3(a) for the PCMs/Se composite, the sharp diffraction peaks of bulk crystalline Se disappear entirely compared to elemental Se, which is suggesting that dispersion of amorphous Se at a molecular level confined in the pores of PCMs. [24] Raman patterns of CMs (black), PCMs (blue) and PCMs/Se (purple) composites are shown in Fig. 3(b). As for the CMs, two broad peaks at around 1350 cm^{-1} and 1580 cm^{-1} are well known as the D band and G band for carbon. The defective nature of the materials is reflected from the intensity ratio ($R = I_D / I_G$) in Raman spectra. The R value of CMs, PCMs, PCMs/Se is 0.92, 0.94 and 0.96 respectively. Obviously, the I_D/I_G of PCMs is higher than CMs, which may dues to more defects and highly porous structures on the PCMs after KOH processing. [25] The XPS spectra of C 1s and Se 3d of PCMs/Se are shown in Fig. 3(c-d). The asymmetry of the C 1s peak which is around 284.8 eV of the PCMs/Se composite in Fig. 3(c) indicates the co-existence of sp^2 and sp^3 carbons owing to the graphitic structure of the carbon matrix. [26] In addition, Fig. 3(d) shows that the position of the Se $3d_{3/2}$ and Se $3d_{5/2}$ peak located at about 56.1 eV and 55.3 eV, which indicating that the strong interaction between Se molecules and PCMs hosts.[27] From the Fig. 3(d), the peak of around 59 eV may come from the bond by Se–C.[28]

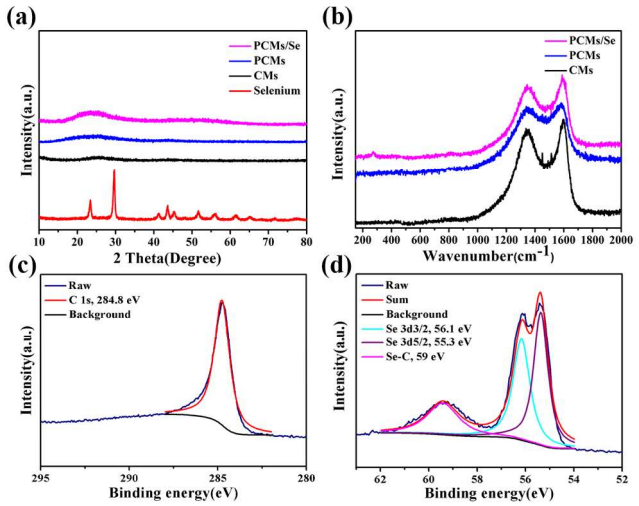

Figure 3 (a) XRD profiles of CMs (black), PCMs (blue), PCMs/Se (purple) and selenium (red). (b) Raman spectra of CMs (black), PCMs (blue), PCMs/Se (purple). XPS of carbon (c) and Se (d) of PCMs/Se composite.

Nitrogen adsorption–desorption tests were used to further examine the surface and characterize the pore size of the samples. Fig. 4(a) shows the BET isotherms curves of the CMs, PCMs and PCM/Se and the specific surface area of CMs is 123.9 m^2 g^{-1} (Table 1). From Fig. 4(b) and Table 1, the surface area of PCMs and its pore-size distribution could be revealed. The surface area of PCMs is 2442.1 m^2 g^{-1}, which is much larger than that of the CMs. After loading Se, the BET surface area of PCMs/Se (Table 1) decreases to 174.1 m^2 g^{-1}, accompanied by a significantly reduction in pore volume distribution, which may due to immersion of Se into porous carbon materials[25]. It is consistent well with our TEM and EDS results. Additionally, the pore size distribution for PCMs is from 1~4 nm, which obviously demonstrated the smaller pore size compared with the CMs. That may because after the KOH activation, the PCMs revealed the better mesoporous structure (1~4 nm). Furthermore, thermogravimetric analysis toward the PCMs/Se composite was carried out under N_2 atmosphere (Fig. 4c) so as to confirm the content of selenium. There is only one weight loss stage observed in the TGA pattern above. From temperature about 390 °C to 530 °C, the mass loss of Se in PCMs/Se composite is determined to be ~52 wt%[29].

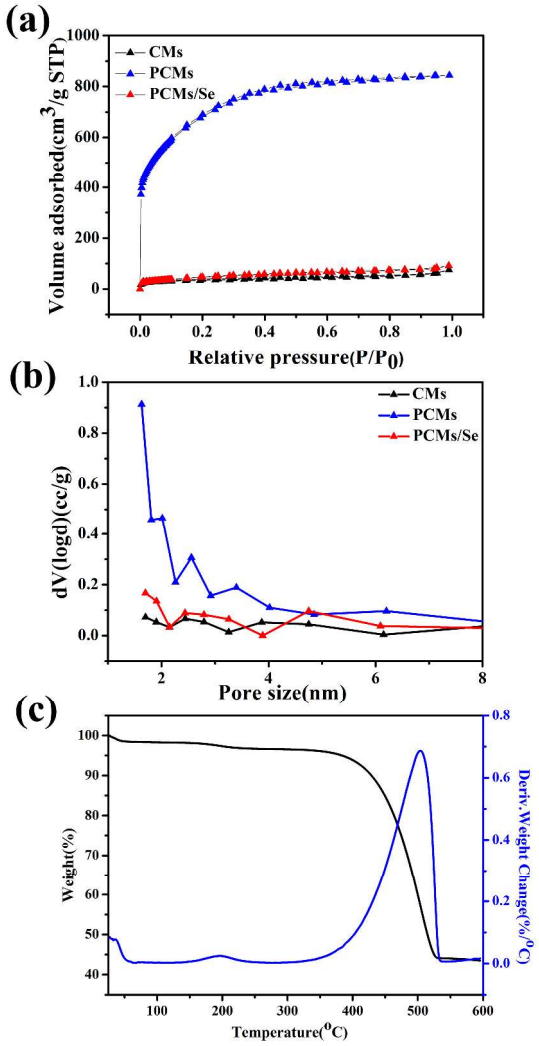

Figure 4 N_2 adsorption-desorption isotherms (a) and the pore size distributions (b) for distinct samples: CMs sample, PCMs and the PCMs/Se composite. (c) TG curves of PCMs/Se under N_2 at a heating rate of 10 ℃ min^{-1}.

Table 1. Porosity properties for CMs, PCMs and PCMs/Se.

sample name	BET area (m^2/g)	pore volume (cc/g)	Pore size (nm)
CMs	123.9	0.12	2~10
PCMs	2442.1	1.31	1~4
PCMs/Se	174.1	0.15	2~6

Electrochemical Performance

CV measurements of the composite PCMs/Se were performed at a scan rate of 0.2 mV s^{-1} from the 1st to 10th cycle and shown in Fig. 5(a). In the figure, for the redox process, only one reduction peak and one oxidation peak can be observed. The reduction peak at 1.7 V is attributed to the direct phase change from Se to Li_2Se and the oxidation peak at 2.2 V corresponds to the conversion from Li_2Se to Se, which indicating that there is no soluble Li_2Se_n ($n \geq 4$) formed during the reaction[29]. The charge-discharge profile of

PCMs/Se composite was shown in Fig. 5(b) with the current density of 0.5 C (1C=675 mA g^{-1}). The excellent performance had been revealed with the initial capacity of about 470 mAh g^{-1}. Any more, the PCMs/Se composite used as the cathode still showed more than 400 mAh g^{-1} capacity

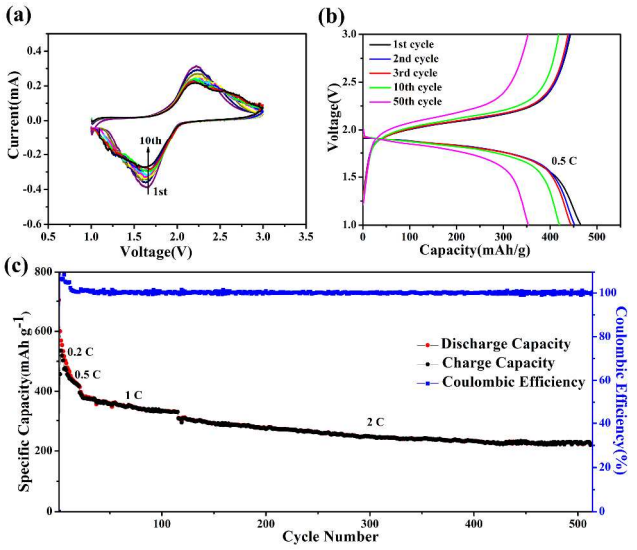

Figure 5 (a) CV curves of the PCMs/Se cathode in a coin cell at a scan rate of 0.2 mV s^{-1}. (b) Charge-discharge profiles of PCMs/Se at different cycle numbers at a rate of 0.5 C (1C=675 mA g^{-1}) and its (c) Rate performance of the PCMs/Se composite cathode under different current rates.

after 10 cycles. All capacities in this study were calculated based on Se mass. For the PCMs/Se composites, a remarkable rate performance is also obtained (Fig. 5c). It exhibits that the specific discharge capacities of PCMs/Se composite, decreasing gradually with the increasing current densities. The cell was operated at four different current densities of 0.2 C, 0.5 C, 1 C and 2 C in a voltage window of 1~3 V, respectively. There was an unconspicuous decline of capacity for 1 C and 2 C, compared to 0.2 C and 0.5 C, this is probably due to the rapid charge–discharge process at a relatively high constant rate, where polyselenides are not immediately dissolved in the electrolyte with the adsorption effect of the interconnected mesopores in PCM so that the shuttle effect is suppressed.[16] After 510 cycles at 2 C, a satisfactory capacity of 230 mAh g^{-1} could be obtained for PCMs/Se composite. Comparison with CMs/Se and CMK-3/Se composite, the discharge capacity is only about 40 mAh g^{-1} and 60 mAh g^{-1} after 100 cycles respectively at a current density of 1 C (Fig. S2).The excellent rate performance of PCMs/Se composite could be ascribed to well electronic conductivity of PCMs and the uniform dispersion of Se in interconnected structure of PCMs matrix.

Conclusions

The composite of Se and rich porous carbon materials with the high surface areas up to 2442.1 m^2 g^{-1} using silkworm cocoon as precursors is explored as cathode for Li-Se batteries for the first time. The high BET specific surface area and abundant pores textures of PCMs become the basic condition as the host matrix of Se reservoir. The composite with highly dispersed state of Se in the PCMs host matrix used as the electrodes exhibit excellent electrochemical performance which may be due to abundant Se loading into the mesopores of PCMs and restraining the dissolution of polyselenides into Li-Se battery electrolytes. We believe that the results here described may substantially contribute to the progress of the Li-Se batteries technology.

Acknowledgements

This work is financially supported by National Program on Key Basic Research Project of China (973 Program) under contract No.2013CB127804. Chongqing Key Laboratory for Advanced Materials and Technologies of Clean Energies under cstc2011pt-sy90001.The work is supported by grants from Fundamental Research Funds for the Central Universities (SWU 113079, XDJK2014C051). Z. S. Lu would like to thank the supports by the Specialized Research Fund for the Doctoral Program of Higher Education (RFDP) (Grant No. 20130182120025), Young Core Teacher Program of the Municipal Higher Educational Institution of Chongqing and Chongqing Natural Science Foundation (cstc2015jcyjA50031).

Notes and references

[a]*Institute for Clean Energy & Advanced Materials, Faculty of Materials and Energy， Southwest University, Chongqing 400715, P.R. China*
[b]*Chongqing Key Laboratory for Advanced Materials and Technologies of Clean Energies, Chongqing 400715, P.R. China*
** Corresponding author*
Fax: +86-23-68254969; Tel: +86-23-68254969;
E-mail: xumaowen@swu.edu.cn; zslu@swu.edu.cn.

1 L. Chen, Y. Zhang, C. Lin, W. Yang, Y. Meng, Y. Guo, M. Li, D. Xiao, *J. Mater. Chem. A*, 2014, **2**, 9684–9690.
2 J. Wang, Y-S. He, J. Yang, *Adv. Mater*. 2015, **27**, 569–575.
3 C-P. Yang, Y-X. Yin, Y-G. Guo, *J. Phys. Chem. Lett.* 2015, **6**, 256−266.
4 V. Etacheri, R. Marom, R. Elazari, G. Salitra, D. Aurbach, *Energy Environ. Sci,* 2011, **4**, 3243–3262.
5 K. A. See, Y-S. Jun, J. A. Gerbec, J. K. Sprafke, F. Wudl, G. D. Stucky, R. Seshadri, *Appl. Mater. Interfaces,* 2014, **6**, 10908−10916.
6 K. Han, Z. Liu, H. Ye, F. Dai, *J. Power Sources*, 2014, **263**, 85-89.
7 B. Zhang, M. Xiao, S. Wang, D. Han, S. Song, G. Chen, Y. Meng, *Appl. Mater. Interfaces,* 2014, **6**, 13174−13182.
8 H. Ye, Y-X. Yin, S-F. Zhang, Y-G. Guo, *J. Mater. Chem. A*, 2014, **2**, 13293–13298.
9 J. Zhang, Y. Xua, L. Fan, Y. Zhu, J. Liang, Y. Qian, *Nano Energy*, 2015, **13**, 592–600.
10 Z. Yi, L. Yuan, D. Sun, Z. Li, C. Wu, W. Yang, Y. Wen, B. Shan, Y. Huang, *J. Mater. Chem. A*, 2015, **3**, 3059–3065.

11 Y. Qu, Z. Zhang, Y. Lai, Y. Liu, J. Li, *Solid State Ionics*, 2015, **274**, 71–76.
12 Z. Zhang, Z. Zhang, K. Zhang, X. Yang, Q. Li, *RSC Adv*, 2014, **4**, 15489–15492.
13 Z. Li, L. Yuan, Z. Yi, Y. Liu, Y. Huang, *Nano Energy*, 2014, **9**, 229–236.
14 J. Zhang, L. Fan, Y. Zhu, Y. Xu, J. Liang, D. Wei, Y. Qian, *Nanoscale*, 2014, **6**, 12952–12957.
15 J. T. Lee, H. Kim, M. Oschatz, D-C. Lee, F. Wu, H-T. Lin, B. Zdyrko, W. I. Cho, S. Kaskel, G. Yushin, *Adv. Energy Mater.* 2014, 1400981.
16 Y. Qu, Z. Zhang, S. Jiang, X. Wang, Y. Lai, Y. Liu, J. Li, *J. Mater. Chem. A*, 2014, **2**, 12255–12261.
17 J. Zhang, Y. Xu, L. Fan, Y. Zhu, J. Liang, Y. Qian, *Nano Energy*, 2015, **13**, 592–600.
18 K. Han, Z. Liu, H. Ye, F. Dai, *J. Power Sources*, 2014, **263**, 85-89.
19 R. Fang, G. Zhou, S. Pei, F. Li, H-M. Cheng, *Chem. Commun*, 2015, **51**, 3667-3670.
20 Z. Zhang, X. Yang, X. Wang, Q. Li, Z. Zhang, *Solid State Ionics*, 2014, **260**, 101–106.
21 C. Luo, Y. Xu, Y. Zhu, Y. Liu, S. Zheng, Y. Liu, A. Langrock, C. Wang, *ACS Nano*, 2013, **9**, 8003-8010.
22 J. Zhang, Z. Zhang, Q. Li, Y. Qu, S. Jiang, *J. Electrochen. Soc*, 2014, **161**, A2093-A2098 .
23 J. Li, X. Zhao, Z. Zhang, Y. Lai, *J. Alloys Compd*, 2015, **619**, 794–799.
24 L. Zeng, X. Wei, J. Wang, Y. Jiang, W. Li, Y. Yu, *J. Power Sources* , 2015, **281**, 461-469.
25 L. Zeng, W. Zeng, Y. Jiang, X. Wei, W. Li, C. Yang , Y. Zhu, Y. Yu, *Adv. Energy Mater*, 2014, 1401377.
26 C. Luo, J. Wang, L. Suo, J. Mao, X. Fan, C. Wang, *J. Mater. Chem. A*, 2015, **3**, 555–561.
27 H. Ye, Y-X. Yin, S-F. Zhang, Y-G. Guo, *J. Mater. Chem. A*, 2014, **2**, 13293–13298.
28 Z. Li, L. Yuan, Z. Yi, Y. Liu, Y. Huang, *Nano Energy*, 2014, **9**, 229–236.
29 C. Wu, L. Yuan, Z. Li, Z. Yi, R. Zeng, Y. Li, Y. Huang, *Sci. China Mater*, 2015, **58**, 91–97.